

ISSN: 0095-8972 (Print) 1029-0389 (Online) Journal homepage: <http://www.tandfonline.com/loi/gcoo20>


Four chromophores in one building block: synthesis, structure and characterization of $\text{trans-[Ru(MQ)}_4\text{Cl}_2\text{]}^{4+}$ and $\text{trans-[Ru(4,4'-bpy)}_4\text{Cl}_2\text{]}$ (MQ⁺ = N-methyl-4,4'-bipyridinium, bpy = bipyridine)

Alejandro Cadranel & José H. Hodak


To cite this article: Alejandro Cadranel & José H. Hodak (2015) Four chromophores in one building block: synthesis, structure and characterization of $\text{trans-[Ru(MQ)}_4\text{Cl}_2\text{]}^{4+}$ and $\text{trans-[Ru(4,4'-bpy)}_4\text{Cl}_2\text{]}$ (MQ⁺ = N-methyl-4,4'-bipyridinium, bpy = bipyridine), Journal of Coordination Chemistry, 68:8, 1452-1464, DOI: [10.1080/00958972.2015.1014351](https://doi.org/10.1080/00958972.2015.1014351)

To link to this article: <http://dx.doi.org/10.1080/00958972.2015.1014351>

 View supplementary material 

 Accepted author version posted online: 06 Feb 2015.
Published online: 24 Feb 2015.

 Submit your article to this journal 

 Article views: 36

 View related articles 

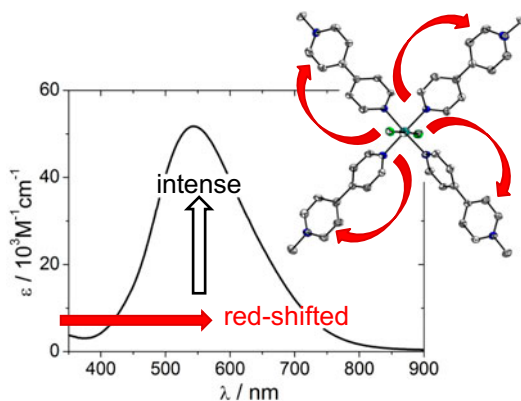
 View Crossmark data 

Four chromophores in one building block: synthesis, structure and characterization of $trans$ -[Ru(MQ)₄Cl₂]⁴⁺ and $trans$ -[Ru(4,4'-bpy)₄Cl₂] (MQ⁺ = N-methyl-4,4'-bipyridinium, bpy = bipyridine)

ALEJANDRO CADRANEL* and JOSÉ H. HODAK*

Departamento de Química Analítica, Inorgánica y Química Física, INQUIMAE, Facultad de Ciencias Exactas y Naturales, Universidad de Buenos Aires, Buenos Aires, Argentina

(Received 14 August 2014; accepted 12 January 2015)



We report the synthesis, crystal structure, electrochemical and spectroscopic properties of $trans$ -[Ru(MQ)₄Cl₂]⁴⁺ (**1**⁴⁺), where MQ⁺ = N-methyl-4,4'-bipyridinium. The crystal structure of **1**⁴⁺ shows the pyridinic rings bound in a $trans$ fashion to the Ru ion. In **1**⁴⁺ and in its analog $trans$ -[Ru(4,4'-bpy)₄Cl₂] (**2**, bpy = bipyridine), the electrochemical reduction waves of the four iminic ligands occur at very closely spaced potentials. In comparison with previously reported analogues, **1**⁴⁺ and **2** present high molar extinction coefficients ($\epsilon = 20,000$ – $50,000 \text{ M}^{-1}\text{cm}^{-1}$), and red-shifted absorptions (up to 800 nm for **1**⁴⁺ and up to 600 nm for **2**) in acetonitrile. Upon protonation of the four exposed nitrogens of **2** and electrochemical reduction of the ligands in **1**⁴⁺ and **2**, spectral changes occur with retention of isosbestic points, revealing the presence of four independent chromophores. These results suggest poor electronic communication between the aromatic ligands within each compound, in contrast to related complexes such as cis -[Ru(2,2'-bpy)₂Cl₂] (**3**).

Keywords: Ruthenium tetrapyrridine; N-methyl-4,4'-bipyridinium; Supramolecular building block; Red sensitization

*Corresponding authors. Email: acadranel@qi.fcen.uba.ar (A. Cadranel); jhodak@qi.fcen.uba.ar (J.H. Hodak)

1. Introduction

Coordination compounds play an important role in supramolecular chemistry [1–13], because metal-based fragments offer diversity and versatility of both structures and functions. Ruthenium tetrapyrindines are attractive building blocks, with the advantage of preserving their *trans* configuration upon substitution of their axial ligands [14, 15], enabling architectures with a thermally and photochemically stable, defined linear geometry. Moreover, derivatization of the pyridine ligands enables them to perform specific functions [16–18] or tune the properties of the systems [19–21]. These fragments have been used as central units in X-Ru(py)₄-Y systems to study electron communication between remote sites [19, 20, 22, 23] and to prepare molecular wires [24, 25]; fields in which linear geometries are preferred because they prevent bending vibrations that alter donor-acceptor distances.

However, reported ruthenium tetrapyrindines are far from being appealing chromophores for sunlight energy applications, and thus they have not been exploited as such. In contrast with the structurally related and more frequently studied ruthenium bis-2,2'-bipyridine complexes [26], Ru(py)₄ moieties do not show absorption features on the red side of the spectrum [27], which are desirable in photo-activated devices [28–30]. Furthermore, the reduction processes of the pyridines occur at very negative potentials and they are not experimentally accessible in regular solvents, unlike bipyridine reductions in Ru(2,2'-bpy)₂ analogs. This precludes the study of the absorption spectrum of the ligand reduced species through spectroelectrochemical techniques, which is considered as a key tool to interpret transient absorption profiles of charge transfer excited states [31]. Given the relevance of the dynamics of charge-separated excited states in energy conversion, this is another discouraging property of Ru(py)₄ complexes. Despite of these drawbacks, there is a distinctive characteristic of ruthenium tetrapyrindines that can be advantageous for sunlight energy harvesting. These complexes formally bear four chromophoric Ru-py pairs, while there are only two Ru-bpy absorbers in their Ru(2,2'-bpy)₂ analogs. This higher chromophoric density (chromophores per metallic ion) is reflected in enhanced molar extinction coefficients for Ru(py)₄ against Ru(2,2'-bpy)₂ dichloro- [32, 33], dicyano- [32, 34], and dihexacyanoferrate- [19] compounds.

The goal of this study is to combine the favorable structural aspects of tetrapyrindinic moieties with the energetics of Ru(2,2'-bpy)₂ complexes, to give supramolecular building blocks useful in sunlight collection. To this end, we have synthesized and characterized *trans*-[Ru(MQ)₄Cl₂]⁴⁺ (**1**⁴⁺) and *trans*-[Ru(4,4'-bpy)₄Cl₂] (**2**) (see figure 1), incorporating into a Ru(py)₄ scaffold the MQ⁺ and 4,4'-bpy ligands. These aromatic heterocycles bear an extended conjugation analogous to that of 2,2'-bpy, so **1**⁴⁺ and **2** are expected to present red-shifted absorption profiles combined with the high molar extinction coefficients, from Ru(py)₄. Experimentally accessible reduction processes would also be expected, as they are typical for bis-2,2'-bipyridines. Compounds **1**⁴⁺ and **2** contain labile chloride ligands as convenient binding sites for further supramolecular connectivity. Comparative analyses are made using *cis*-[Ru(2,2'-bpy)₂Cl₂] (**3**) and *trans*-[Ru(py)₄Cl₂] (**4**) as reference compounds (figure 1).

2. Experimental

2.1. Materials and physical measurements

[Ru(DMSO)₄Cl₂] [35], N-methyl-4,4'-bipyridinium iodide (MQI) [36] and *trans*-[Ru(4,4'-bpy)₄Cl₂] [37] (**2**) were prepared according to previous reports. MQPF₆ was obtained by

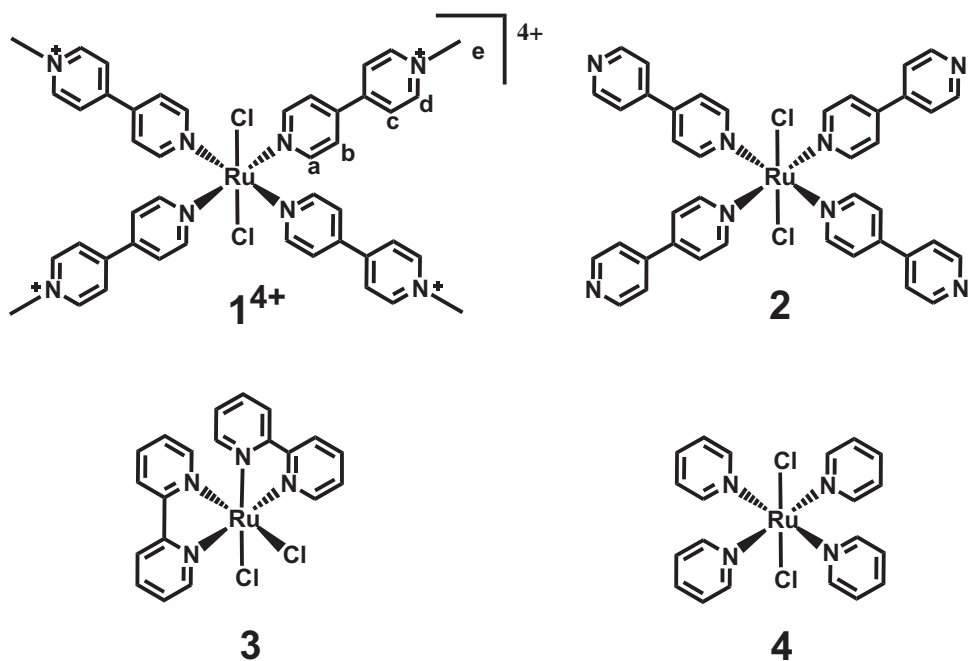


Figure 1. Structure of $trans-[Ru(MQ)_4Cl_2]^{4+}$ (**1**⁴⁺), $trans-[Ru(4,4'-bpy)_4Cl_2]$ (**2**), $cis-[Ru(2,2'-bpy)_2Cl_2]$ (**3**) and $trans-[Ru(py)_4Cl_2]$ (**4**). Labels identify hydrogen atoms according to NMR assignments.

anion interchange, dissolving MQI in hot water, adding a 20% excess of KPF_6 and filtering the white solid material. Solvents for electrochemical, spectral, and spectroelectrochemical measurements were dried using a PureSolv Micro solvent purification system. All other reagents were obtained commercially and used as supplied. The compounds synthesized were dried in a vacuum desiccator over silica gel for at least 12 h prior to characterization. UV–visible spectra were recorded with a Hewlett-Packard 8453 diode array spectrometer (190–1100 nm). 1H NMR spectra were measured with a Bruker ARX500 spectrometer using deuterated solvents from Aldrich. Elemental analyses were done on a Carlo Erba 1108 analyzer with an estimated error of $\pm 0.5\%$. Electrochemical measurements were performed under argon with millimolar solutions of the compounds, using a TEQ V3 potentiostat and a standard three electrode arrangement consisting of a glassy carbon disk (area = 9.4 mm^2) as working electrode, a platinum wire as counter electrode, and a silver wire as reference electrode plus an internal ferrocene (Fc) standard. Tetra-*n*-butylammonium hexafluorophosphate ($[TBA]PF_6$, 0.1 M) was used as the supporting electrolyte. All the potentials reported in this work are referenced to the standard Ag/AgCl saturated KCl electrode (0.197 V *versus* NHE), the conversions being performed with literature values for the Fc⁺/Fc couple [38]. Coulometric analyses were accomplished applying potentials of 1.0 V (oxidation of **1**⁴⁺ and **2**), -1.0 V (first reduction of **1**⁴⁺), -2.0 V (first reduction of **2**), and the total charge calculated by integration of the current *versus* time curve. pH was measured using a Metrohm 744 pH-meter calibrated with standard buffer solutions immediately before measurements. Acidic titration from pH 6.5 to 0.5 was accomplished by adding different aliquots of HCl 1 M, to an aqueous solution of **2**, initially dispersed in a drop of acetone. Absorption spectra were corrected for dilution. Spectroelectrochemical (SEC)

experiments were performed using a three-electrode OTTLE cell [39], with millimolar solutions of the compounds using [TBA]PF₆ 0.1 M as the supporting electrolyte.

2.2. X-ray crystallography

Crystal structure of **1**(PF₆)₄ was determined with an Oxford Xcalibur, Eos, Gemini CCD area-detector diffractometer using graphite-monochromated Mo-K α radiation ($\lambda = 0.71069$ Å) at 298 K. Data were corrected for absorption with CrysAlisPro, Oxford Diffraction Ltd., Version 1.171.33.66, applying an empirical absorption correction using spherical harmonics, implemented in SCALE3 ABSPACK scaling algorithm [40]. The structures were solved by direct methods with SHELXS-97 [41] and refined by full-matrix least-squares on F^2 with SHELXL-97 [41]. Hydrogens were added geometrically and refined as riding atoms with a uniform value of U_{iso} , with the exception of hydrogens of the water molecule, which were not located in the difference map and, hence, were not included in the model. Final crystallographic data and values of R_1 and wR are listed in table S1 (see online supplemental material at <http://dx.doi.org/10.1080/00958972.2015.1014351>), while the main angles and distances are listed in table 1.

2.3. Synthesis of *trans*-[Ru(MQ)₄Cl₂](PF₆)₄ (**1**(PF₆)₄)

150 mg of [Ru(DMSO)₄Cl₂] (0.31 mM) and 1.2 g of MQPF₆ (14 equivalents) were suspended in 100 mL of methanol and heated at reflux for 12 h. After cooling at room

Table 1. Selected bond angles and distances of the crystal structures of **1**(PF₆)₄ and **2**.

Compound	1 (PF ₆) ₄	2 ^a
<i>Distances (Å)</i>		
Ru–N	2.091(7)	2.071(5)
	2.087(7)	2.069(5)
	2.075(6)	2.065(6)
	2.073(6)	2.064(6)
Ru–Cl	2.405(3)	2.411(2)
	2.394(3)	2.398(2)
<i>Angles (°)</i>		
N–Ru–N	90.0(3)	90.0(2)
	89.4(3)	89.2(2)
	88.7(3)	88.6(2)
	88.1(3)	87.8(2)
Cl–Ru–Cl	177.38(9)	179.21(8)
N–Ru–Cl	89.69(19)	89.87(17)
	89.13(19)	89.83(17)
	88.99(19)	89.79(18)
	88.97(19)	89.57(17)
	88.57(19)	89.06(18)
	88.49(19)	88.98(17)
	88.44(19)	88.84(17)
	87.73(19)	88.69(18)
<i>Torsions (°)</i>		
C–N–Ru–Cl	44.39	44.92
	42.95	41.79
	41.97	39.57
	32.85	37.82

^aTaken from Ref. [37].

temperature, a dark solid was collected by filtration from a reddish-brown solution and dissolved in a minimum of acetone. It was loaded on a Al_2O_3 column, also packed in acetone. Elution with acetone/ethanol, with increasing proportions of ethanol, resulted in the removal of the free ligand. To obtain the metal complex, it is necessary to elute with ethanol/methanol mixtures with increasing proportions of methanol. Sometimes, few drops of $\text{HCl}(\text{c})$ are added to the final elution mixture to remove the metal complex. However, this purification method always led to a considerable loss of sample attached to the stationary phase. The violet fractions containing the metal complex were dried and dissolved in a minimum volume of acetone. After one equivalent of KPF_6 was added together with 30 mL of water, a purple solid was collected by filtration, washed with water at room temperature (3×5 mL), and dried. Yield: 196 mg (44%). Anal. Calcd for $\text{C}_{44}\text{H}_{54}\text{O}_5\text{N}_8\text{Cl}_2\text{P}_4\text{F}_{24}\text{Ru}$ (**1** (PF_6) $_4 \cdot 5\text{H}_2\text{O}$): C, 34.6; H, 3.6; N, 7.3. Found: C, 34.4; H, 3.2; N, 7.0. ^1H NMR ($(\text{CD}_3)_2\text{CO}$, 200 MHz, figure S1) δ (ppm): 9.17 (d, 8H, $J=7.0$ Hz, H^{a}), 8.85 (d, 8H, $J=7$ Hz, H^{d}), 8.66 (d, 8H, $J=7$ Hz, H^{b}), 7.91 (d, 8H, $J=7$ Hz, H^{c}), 4.62 (s, 12H, H^{e}).

3. Results and discussion

3.1. Synthesis

Preparation of **1**(PF_6) $_4$ is similar to other ruthenium tetrapyrindines [19], involving $[\text{Ru}(\text{DMSO})_4\text{Cl}_2]$ precursor and 14 times excess of ligand. In this case, purification from the free MQ^+ is not straightforward, and column chromatography with basic Al_2O_3 is required before recrystallization. The resulting solid material shows pure ^1H NMR patterns (figure S1) that indicate equivalency between the four pyridinic ligands and therefore a *trans* configuration. This suggests that linear supramolecular arrangements can be generated upon substitution of chloride ligands. In sunlight energy conversion devices, this geometry is preferred over the *cis* counterpart because it generates a smaller footprint on the surface of sensitized electrodes, allowing for a higher degree of occupation of the surface and, hence, a higher absorbance [42].

3.2. Crystal structure

X-ray quality single crystals of **1**(PF_6) $_4$ were obtained by slow evaporation of a concentrated methanol-acetone solution. The molecular structure of **1** $^{4+}$ was determined by single crystal X-ray diffraction as shown in figure 2. Selected bond distances and angles for **1** $^{4+}$ and **2** are summarized in table 1 (crystallographic data in table S1). Ruthenium ions present octahedral coordination environments, with N-Ru-Cl and N-Ru-N angles averaging between 88.8° and 89.3° , and an almost linear *trans* configuration of chlorides, with a Cl-Ru-Cl angle of 177.38° . Like other ruthenium tetrapyrindinic fragments [19, 20, 43], **1** $^{4+}$ presents a propeller-like configuration of the coordinated pyridinic rings, with an average tilting angle of 40° – 41° . Ru-N bond distances average 2.082 \AA for **1** $^{4+}$, larger than those of **2** (2.067 \AA), due to the electron-withdrawing character of the distant nitrogens upon methylation. As the electron withdrawing character of the quaternary nitrogen in **1** $^{4+}$ makes the pyridinic ligand MQ^+ a weaker σ -donor and a better π -acceptor than 4,4'-bpy, it can be stated that the σ -component of the coordination bond is, in this case, more important than its π -component, and thus the Ru-N bond is weaker and longer with MQ^+ . Establishing a

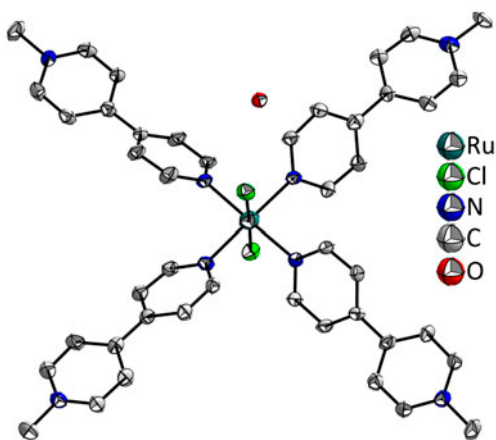


Figure 2. Crystal structure of 1^{4+} . Ellipsoids represent a 30% displacement probability. The oxygen belongs to a water of solvation. Hydrogens and $(PF_6)^-$ counter ions were omitted for clarity.

general relationship between pyridine basicity (or its ability towards σ -bonding) and Ru–N bond distance might be appealing. However, the few structures of tetrapyridine-dichloro ruthenium moieties reported do not show a clear trend on these parameters [44, 45]. For example, 3-methylpyridine is more basic than pyridine, but it comprises longer Ru–N distances. This means that in some cases π -interactions may play a significant role.

Compound 1^{4+} crystallizes with one solvation water molecule, which is involved in chains of molecules connected by RuCl–O–ClRu sequences. Chains are not interconnected by any stacking and counterions are placed in the void spaces between chains. In contrast, the structure of **2** does not include any solvation molecule and presents double-stacking (3.43 Å) between two ligands of each molecule. This originates dimeric fragments interconnected by a short contact (2.86 Å) between the chloride and an ortho hydrogen of the coordinating pyridinic ring. Ru–Cl distances average 2.40 Å for both 1^{4+} and **2**, and are similar to related analogs [44, 45], so in this case packing interactions are not geometry-determining.

Unfortunately, hydrogens could not be refined for the solvation water molecule of 1^{4+} , precluding an unequivocal evaluation of Cl–O–Cl interactions as hydrogen bonded (Cl \cdots H–O) or halogen bonded (Cl \cdots O) [46–48]. Although Cl–O distances (3.13 and 3.22 Å) are shorter than the sum of their Van der Waals radii, which makes the presence of a collinear hydrogen atom between them unlikely, similar distances have been observed for the crystal structure of *cis*-[Ru(bpy) $_2$ Cl $_2$] \cdot 3.5H $_2$ O.⁴⁹ In that structure, almost collinear hydrogen atoms could be effectively refined and a H-bonded structure was proposed, with a Cl \cdots H–O angle of 164°. However, whereas for the bpy compound the Cl \cdots O \cdots Cl angle is 102°, in the case of 1^{4+} it takes the value of 78.52°, which is unusually small for a water molecule. Halogen bonding is indeed expected to occur in molecular arrangements carrying a polarizable halogen, such as iodine or bromine attached to an electron withdrawing moiety. In such cases, directional distortion of the electronic density at the halogen results in an electron deficiency, and oxygen can act as a donor towards this electron-poor region [48]. Despite of chloride being appreciably less polarizable than the heavier halogens, the reduction potential of the Ru(III/II) couple as well as the energy of electronic transitions in 1^{4+} strongly

suggests that this metal center is electron deficient (*vide infra*). Therefore, we postulate the possible occurrence of halogen bonds in the crystal structure of $\mathbf{1}^{4+}$. Other dichloro analogs will be prepared in our labs in order to confirm this hypothesis.

3.3. Electrochemical measurements

The electrochemical measurements for $\mathbf{1}^{4+}$ and $\mathbf{2}$ in DMSO shown in figure 3 and table 2 present similar features. Both compounds have one wave at anodic potentials, ascribable to a metal-centered oxidation i.e. the ruthenium(III/II) couple, which is irreversible in the case of $\mathbf{1}^{4+}$. The oxidized species $\mathbf{1}^{5+}$ is not available for electrochemical reduction on the electrode surface, owing to chemical reaction with traces of solvent impurities or precipitation processes favored by the high state of charge. Due to the enhanced acceptor character of MQ^+ ligands with respect to 4,4'-bpy, the Ru(III)/(II) process shifts anodically by 200 mV for $\mathbf{1}^{4+}$. The different charge, +4 for $\mathbf{1}^{4+}$ and 0 for $\mathbf{2}$, may also contribute in stabilizing the Ru(II) oxidation state in $\mathbf{1}^{4+}$. Additionally, cathodic scans reveal two quasi-reversible processes for each complex, anodically shifted in the case of $\mathbf{1}^{4+}$. As previously seen for the free ligands [50] and related compounds [37, 51, 52], these waves are assigned to ligand-centered consecutive reductions, i.e. the 4,4'-bpy/(4,4'-bpy) $^-$ and (4,4'-bpy) $^-$ /(4,4'-bpy) $^{2-}$ couples, for example.

Reduction of individual ligands in $\mathbf{1}^{4+}$ and $\mathbf{2}$ occurs at such closely spaced potentials that they could not be resolved by either of the electrochemical methods employed. Coulometric measurements render $n_{\text{red}}/n_{\text{ox}}$ ratios of 4.4 for $\mathbf{1}^{4+}$ and 4.2 for $\mathbf{2}$ ($n_{\text{red/ox}}$ = charge equivalents involved in the reduction/oxidation process), showing that each of the observed cathodic signals accounts for four electrons. This phenomenon is not unexpected, as it has already been found for complexes containing two MQ^+ ligands [53–55], and it suggests that electronic communication between the ligands of each molecule is poor. In contrast to this behavior, $\mathbf{3}$ [56], $[\text{Ru}(\text{bpy})_3]^{2+}$ [57], and other ruthenium polypyridines [58] present clearly resolved ligand-centered, one-electron reduction processes arising from ligand–ligand electronic communication to a much higher extent. This difference in redox properties is entirely analogous to that for the bimetallic compounds $[\{\text{Ru}(2,2'\text{-bpy})_2\text{Cl}\}_2(\mu\text{-B})]^{2+}$ (B = bridging ligands). When B is 4,4'-bpy, both ruthenium ions are oxidized in a single

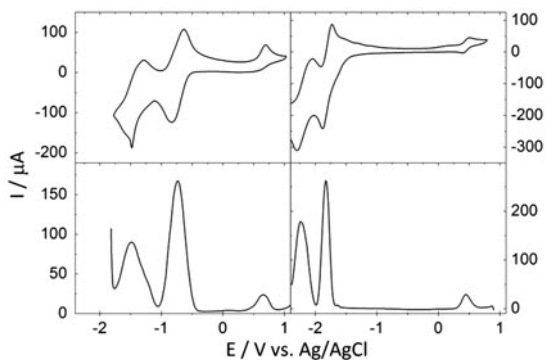


Figure 3. Cyclic voltammograms of $\mathbf{1}^{4+}$ (left) and $\mathbf{2}$ (right) in DMSO/0.1 M [TBA]PF $_6$ at 100 mV s $^{-1}$ (upper panel), and differential pulse voltammograms of $\mathbf{1}^{4+}$ (left) and $\mathbf{2}$ (right) in DMSO/0.1 M [TBA]PF $_6$ at a pulse frequency of 2 Hz and an amplitude of 50 mV, with a staircase step of 10 mV (bottom panel).

Table 2. Electrochemical and spectroscopic data for $\mathbf{1}^{4+}$, $\mathbf{2}$, $\mathbf{H}_4\mathbf{2}^{4+}$, $\mathbf{3}$, $\mathbf{4}$ and the free ligands MQ^+ and 4,4'-bpy.

Complex	Solvent	$E_{1/2} (\Delta E_p)/V$ (mV) ^a			$\lambda_{\text{max}}/\text{nm}$ ($\epsilon_{\text{max}}/10^3 \text{ M}^{-1} \text{ cm}^{-1}$)	
		Ru(III/II)	L/L ⁻	L ⁻ /L ²⁻	LC $\pi \rightarrow \pi^*$	MLCT $d\pi(\text{Ru}) \rightarrow \pi^*(\text{L})$
1	DMSO	0.66 ^f	-0.74 (200)	-1.49 (240)	266 (121)	545 (51.8)
	CH ₃ CN					
	H ₂ O					
2	DMSO	0.45 (90)	-1.85 (150)	-2.25 (230)	258 (110)	501 (47.6)
	CH ₃ CN					
	H ₂ O					
H₄2⁴⁺	H ₂ O				247 (46.1)	458 (23.4)
3^b	H ₂ O	0.32 (70)	-1.67 ^f	na	249 (71.4)	443 (31.5)
	CH ₃ CN					
4^c	H ₂ O	0.32 (70)	-1.78 ^f	na	258 (88.9)	486 (38.3)
	CH ₃ CN					
MQ^{+d}	H ₂ O	0.31 (80)	na	na	243 (21.0)	380 (8.90)
	CH ₃ CN					
4,4'-bpy ^e	H ₂ O	0.31 (80)	na	na	297 (50.0)	553 (9.10)
	CH ₃ CN					
					250 (15.7)	398 (25.1)
						450 (7.80) sh

^a0.1 M [TBA]PF₆ used as electrolyte.^bFrom Ref. [56].^cFrom Ref. [32].^dFrom Ref. [52].^eFrom Ref. [37].^fIrreversible.

two-electron process [53], whereas if B is a shorter bridge as pyrazine, more likely to promote metal–metal interactions, two separated one-electron waves are observed [59].

3.4. UV–vis spectroscopy

The electronic absorption spectra of $\mathbf{1}^{4+}$ and $\mathbf{2}$ in acetonitrile are shown in the left panel of figure 4 and relevant data are collected in table 2. Both complexes present one ligand-centered (LC) transition in the UV and one metal-to-ligand charge transfer (MLCT) band in the visible. This simple pattern of signals resembles the spectroscopy of $\mathbf{4}$ [15]. However, MQ^+ and 4,4'-bpy present a more pronounced π acceptor character than pyridine due to the extended conjugated π system over the iminic ligands, thus the MLCT bands of $\mathbf{1}^{4+}$ and $\mathbf{2}$

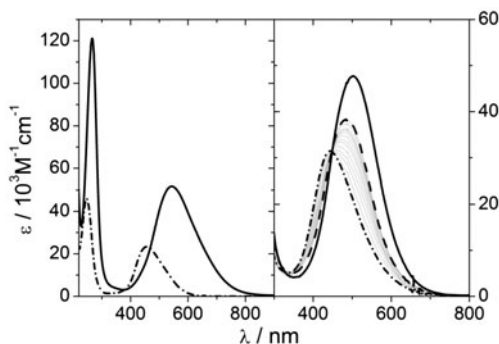


Figure 4. Left panel: UV–vis absorption profiles in acetonitrile of $\mathbf{1}^{4+}$ (solid line) and $\mathbf{2}$ (dashed-dotted line). Right panel: UV–vis absorption profiles in water of $\mathbf{1}^{4+}$ (solid line), $\mathbf{2}$ (dashed-dotted line) and the fully protonated species $\mathbf{H}_4\mathbf{2}^{4+}$ (dashed line). Thin gray lines show the spectral evolution of $\mathbf{2}$ during acidic titration.

are red-shifted in comparison with **4**. In this sense, electronic absorption features of **1**⁴⁺ and **2** approach those of **3**, which bear 2,2'-bpy ligands also with an extended conjugated system, although the lower symmetry of **3** results in a splitting of the MLCT absorptions in two sets of bands [60]. **1**⁴⁺ and **2** present higher chromophoric density than **3**, and thus they show higher molar extinction coefficients. Their absorptivities, around 50×10^3 and $25 \times 10^3 \text{ M}^{-1} \text{ cm}^{-1}$ for **1**⁴⁺ and **2**, respectively, are important in comparison with N3, Z907 and other ruthenium polypyridinic dyes operating in performing dye-sensitized solar cells, usually ranging $10\text{--}45 \times 10^3 \text{ M}^{-1} \text{ cm}^{-1}$ [61]. They are also similar to those of bimetallic compounds ($37 \times 10^3 \text{ M}^{-1} \text{ cm}^{-1}$) [62] and tetrametallic dendrimers ($40 \times 10^3 \text{ M}^{-1} \text{ cm}^{-1}$) [63]. Hence, the supramolecular systems prepared with **1**⁴⁺ and **2** as building blocks would be able to reach high absorptivities with a reduced amount of material. More importantly, the use of multichromophoric building blocks would greatly facilitate the synthetic work needed. We believe that this makes these complexes attractive for sunlight harvesting endeavors.

Methylation of the free nitrogens of **2** results in a stabilization of the ligand π^* LUMO [50] in **1**⁴⁺ because of the electron withdrawing character of the quaternary iminic group. Consequently, the $\pi(\text{MQ}) \rightarrow \pi^*(\text{MQ})$ transition in **1** (266 nm) is red-shifted with respect to the $\pi(\text{bpy}) \rightarrow \pi^*(\text{bpy})$ transition in **2** (247 nm). The stabilization effect is less pronounced on the $d\pi$ orbitals of the metal center, hence the $d\pi(\text{Ru}) \rightarrow \pi^*(\text{MQ})$ band (545 nm) in **1** is also red-shifted compared to the $d\pi(\text{Ru}) \rightarrow \pi^*(\text{bpy})$ charge transfers (458 nm) in **2** (table 2 and figure 4, left panel). For similar reasons, protonation of the bipyridines in **2** (here and in related complexes, $\text{pK}_a(4,4'\text{-bpy}) \sim 4.1$) [64, 65] also produces a red-shift of the spectrum (figure 4, right panel). Note the resemblance of the absorption profile of **1**⁴⁺ in water (solid curve) with that for the fully protonated **H**₄**2**⁴⁺ species (dashed curve). The right panel of figure 4 shows the pH dependence (thin lines) of the absorption spectrum of **2** (dashed-dotted curve) in water, where decreasing the pH promotes displacements of 10 and 40 nm for the LC transition and the MLCT band, respectively.

Remarkably, these absorption changes proceed with retention of two isosbestic points at 337 and 447 nm. These guarantees there are only two absorbing species involved in the acid–base equilibrium, which we interpret as the unprotonated (Ru(bpy)) and protonated (Ru(Hbpy)) forms of the chromophores. In this model, each molecule of **2** bears four protonatable chromophores, so the absorptivity of any protonation state of **2** can be described as a linear combination of the absorptivities of Ru(bpy) and Ru(Hbpy) fragments:

$$\varepsilon(\text{H}_n\mathbf{2}^{n+}) = (4 - n) \varepsilon(\text{Ru}(\text{bpy})) + n \varepsilon(\text{Ru}(\text{Hbpy})) \quad (1)$$

This additive behavior of the absorption properties constitutes another indication of the small electronic communication between the different pyridinic ligands within a molecule of **2**.

3.5. UV–vis spectroelectrochemistry

UV–vis spectroelectrochemical studies were performed on **1**⁴⁺ and **2**, and the spectral evolution during their first reduction process is shown in figure 5. The reduced form of **1**⁴⁺ shows two absorptions with maxima at 370 and 548 nm (figure 5, left panel, red curve). These features have already been observed in related complexes [53] and have been ascribed to one-electron reduced MQ^+ ligands, because they are similar in shape and energy to those observed with the singly reduced N,N-dimethylbipyridinium [39, 66]. In the case

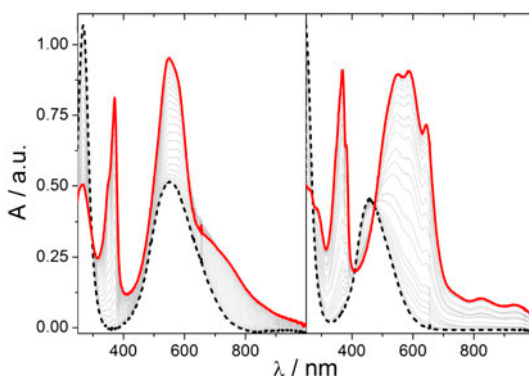


Figure 5. UV-vis spectroelectrochemistry during the first reduction of $\mathbf{1}^{4+}$ (left panel, DMSO, at -1.0 V) and $\mathbf{2}$ (right panel, CH_3CN , at -2.0 V). Initial and final spectra are represented by dashed black and solid red curves, respectively (see <http://dx.doi.org/10.1080/00958972.2015.1014351> for color version).

of $\mathbf{2}$, upon completion of the first reduction a sharp signal at 368 nm appears, together with a broad band centered at 580 nm with defined shoulders and less intense features over 700 nm. This profile is analogous to that reported for singly reduced 4,4'-bpy [50]. These results confirm the assignment of the cathodic signals observed in electrochemical experiments as single reductions of individual ligands.

From the reductive spectroelectrochemistry experiments, isosbestic points for both $\mathbf{1}^{4+}$ (296 nm) and $\mathbf{2}$ (272, 409 and 474 nm) are observed, ensuring there are only two absorbing species taking part in each redox equilibrium. On the basis of their UV-vis profiles we assign them to the regular ($\text{Ru}(\text{L})$) and the one-electron reduced ($\text{Ru}(\text{L}^-)$) forms of the chromophores. This picture is entirely consistent to that for the acid-base equilibrium of $\mathbf{2}$, described in Section 3.4. Here, each molecule of $\mathbf{1}^{4+}$ and $\mathbf{2}$ bears four reducible chromophores, so the absorptivity of any reduction state of $\mathbf{1}^{4+}$ and $\mathbf{2}$ can be described as a linear combination of the absorptivities of the $\text{Ru}(\text{L})$ and $\text{Ru}(\text{L}^-)$ fragments:

$$\varepsilon(\mathbf{Ru}(\mathbf{L})_{4-n}(\mathbf{L}^-)_n) = (4 - n) \varepsilon(\text{Ru}(\text{L})) + n \varepsilon(\text{Ru}(\text{L}^-)) \quad (2)$$

These results further demonstrate that electronic communication between the different pyridinic ligands in $\mathbf{1}^{4+}$ and $\mathbf{2}$ can be considered negligible.

The spectroelectrochemical experiments also provide access to the spectra of the reduced (figure 5, equations (1) and (2) and figure S3) and oxidized (see SI, figures S2 and S3) forms of the chromophores. The sum of their absorption profiles can be used as an approximation of the transient absorption spectra of the MLCT excited states [31], which is very helpful to interpret the excited state ultrafast dynamics of molecular systems bearing these chromophores. The data shown in figure S3 suggest that, in the case of $\mathbf{1}^{4+}$, photoinduced bleach bands should be observed between 420 and 530 nm, and also between 600 and 675 nm, and photoinduced absorption bands are expected in the rest of the spectrum. In $\mathbf{2}$, a photoinduced bleach band should be observed between 400 and 500 nm, while photoinduced absorption signals should appear at both shorter and longer wavelengths. Hence, these results encourage further ultrafast transient absorption studies of larger arrangements containing ruthenium tetrapyrrolic chromophores as sensitizers, which are being undertaken in our labs. This is particularly important for molecules designed to be part of

sunlight conversion systems, such as those presented here. To the best of our knowledge, these are the first reductive spectroelectrochemical results presented for Ru(py)₄-like moieties.

4. Conclusion

The building blocks presented in this work are in-line with current supramolecular strategies for creating light harvesting devices with higher efficiencies. Specifically, **1**⁴⁺ and **2** present a convenient combination of the properties of ruthenium tetrapyrindines and ruthenium polypyridines. The Ru(py)₄ motif provides advantageous structural characteristics for a supramolecular building block, such as a *trans* configuration confirmed by XRD experiments. This can be exploited to prepare sensitized surfaces with denser coverages. The incorporation of the bpy-type extensively conjugated MQ⁺ and 4,4'-bpy ligands results in appealing electronic features typical of Ru(2,2'-bpy)₂, such as MLCT bands well spanned over the visible region reaching 800 nm in **1**⁴⁺ and 600 nm in **2**. Enhanced absorptivity typical of ruthenium tetrapyrindines is preserved in **1**⁴⁺ and **2**, taking values of 50×10^3 and $25 \times 10^3 \text{ M}^{-1} \text{ cm}^{-1}$, respectively. These are high in comparison with ruthenium polypyridines operating in best performing dye-sensitized solar cells ($10\text{--}45 \times 10^3 \text{ M}^{-1} \text{ cm}^{-1}$) and supramolecular systems of higher nuclearity ($35\text{--}40 \times 10^3 \text{ M}^{-1} \text{ cm}^{-1}$), which is a consequence of the high chromophoric density presented by **1**⁴⁺ and **2**.

Electrochemical reduction processes on the ligands were addressed, showing closely spaced reduction potentials of the aromatic heterocycles. To shed light on the nature of these processes, spectroelectrochemical techniques were employed. The evolution of the spectra of **1**⁴⁺ and **2** upon electrochemical reduction, and that of **2** upon free nitrogen protonation, proceed with retention of clear isosbestic points. This is a consequence of negligible electronic coupling between the pyridinic ligands and the presence, in **1**⁴⁺ and **2**, of four independent chromophores per metal ion, one for each Ru-py pair.

Electronic absorption and electrochemical properties of **1**⁴⁺ and **2** encourage further transient absorption studies of the chromophoric fragments presented here. The spectroelectrochemical experiments reported here provide valuable guidance. Taken together, the unique properties discussed here make these complexes attractive supramolecular building blocks for sunlight harvesting.

Supplementary material

CCDC 1018587 contains the supplementary crystallographic data for this paper. These data can be obtained free of charge from the Cambridge Crystallographic Data Center via www.ccdc.cam.ac.uk/data_request/cif.

Acknowledgments

A.C. is a postdoctoral fellow and J.H.H. a member of the scientific staff of CONICET. The authors thank Dr Pablo Alborés for crystal structure refinement, Dr Fabio Cukiernik for fruitful discussions about halogen bonding, and Dr Leonardo Slep for revising this manuscript. A.C. acknowledges ALN for the inspiring brainstorming sessions.

Funding

This work was supported by the University of Buenos Aires (UBA) [grant number UBACYT 01-w971]; the Agencia Nacional de Promoción Científica y Tecnológica (ANPCyT) [grant number PICT-2012-2041], [grant number PICT-2009-107].

References

- [1] M.W. Cooke, G.S. Hanan. *Chem. Soc. Rev.*, **36**, 1466 (2007).
- [2] M.W. Cooke, D. Chartrand, G.S. Hanan. *Coord. Chem. Rev.*, **252**, 903 (2008).
- [3] M. Ferrer, D. Gómez-Bautista, A. Gutiérrez, J.R. Miranda, G. Orduña-Marco, L.A. Oro, J.J. Pérez-Torrente, O. Rossell, P.G. García-Orduña, F.J. Lahoz. *Inorg. Chem.*, **53**, 1699 (2014).
- [4] L. Cola, V. Balzani, P. Belser, R. Dux, M. Baak. *Supramol. Chem.*, **5**, 297 (1995).
- [5] K.E. Splan, A.M. Massari, G.A. Morris, S.-S. Sun, E. Reina, S.T. Nguyen, J.T. Hupp. *Eur. J. Inorg. Chem.*, **2003**, 2348 (2003).
- [6] J.M. Lehn. *Angew. Chem. Int. Ed. Engl.*, **29**, 1304 (1990).
- [7] J.B. Pollock, G.L. Schneider, T.R. Cook, A.S. Davies, P.J. Stang. *J. Am. Chem. Soc.*, **135**, 13676 (2013).
- [8] A. Bahreman, B. Limburg, M.A. Siegler, R. Koning, A.J. Koster, S. Bonnet. *Chem. Eur. J.*, **18**, 10271 (2012).
- [9] Y. Chen, G. Cheng, K. Li, D.P. Shelar, W. Lu, C.-M. Che. *Chem. Sci.*, **5**, 1348 (2014).
- [10] J.M.J. Frechet. *Proc. Natl. Acad. Sci. USA*, **99**, 4782 (2002).
- [11] N. Lanigan, X. Wang. *Chem. Commun.*, **49**, 8133 (2013).
- [12] V. Balzani, L. De Cola, L. Prodi, F. Scandola. *Pure Appl. Chem.*, **62**, 1457 (1990).
- [13] V. Balzani, F. Barigelletti, L. Cola. *Top. Curr. Chem.*, **158**, 31 (1990).
- [14] T. Sheng, H. Vahrenkamp. *Eur. J. Inorg. Chem.*, **2004**, 1198 (2004).
- [15] B.J. Coe, T.J. Meyer, P.S. White. *Inorg. Chem.*, **34**, 3600 (1995).
- [16] M. Biancardo, P.F.H. Schwab, R. Argazzi, C.A. Bignozzi. *Inorg. Chem.*, **42**, 3966 (2003).
- [17] M. Tagliacucchi, L.P. De Leo, A. Cadranell, L.M. Baraldo, E. Völker, C. Bonazzola, E.J. Calvo, V. Zamylny. *J. Electroanal. Chem.*, **649**, 110 (2010).
- [18] K. Naka, A. Kobayashi, Y. Chujo. *Macromol. Rapid Commun.*, **18**, 1025 (1997).
- [19] P. Alborés, L.D. Slep, T. Weyhermüller, L. Baraldo. *Inorg. Chem.*, **43**, 6762 (2004).
- [20] G.E. Pieslinger, P. Albores, L.D. Slep, B.J. Coe, C.J. Timpson, L.M. Baraldo. *Inorg. Chem.*, **52**, 2906 (2013).
- [21] G.E. Pieslinger, B.M. Aramburu-Trošelj, A. Cadranell, L.M. Baraldo. *Inorg. Chem.*, **53**, 8221 (2014).
- [22] M.B. Rossi, K. Abboud, P. Alborés, L.M. Baraldo. *Eur. J. Inorg. Chem.*, **2010**, 5613 (2010).
- [23] M.B. Rossi, P. Alborés, L.M. Baraldo. *Inorg. Chim. Acta*, **374**, 334 (2011).
- [24] P. Alborés, L.D. Slep, L.S. Eberlin, Y.E. Corilo, M.N. Eberlin, G. Benítez, M.E. Vela, R.C. Salvezza, L.M. Baraldo. *Inorg. Chem.*, **48**, 11226 (2009).
- [25] G.E. Pieslinger, P. Alborés, L.D. Slep, L.M. Baraldo. *Angew. Chem. Int. Ed.*, **53**, 1293 (2014).
- [26] A. Juris, V. Balzani, F. Barigelletti, S. Campagna, P. Belser, A. von Zelewsky. *Coord. Chem. Rev.*, **84**, 85 (1988).
- [27] Reported Ru(py) systems include 4-alkyl, 4-methoxy and 4-dimethylamino groups, whose absorption band maxima appear under 400 nm. Nevertheless, a red-shift was accomplished by substituting the pyridines in the 4-position with electron withdrawing groups in [Ru(methylisonicotinate)₄Cl₂], that absorbs at 460 nm [18].
- [28] V. Balzani, A. Credi, M. Venturi. *Molecular Devices and Machines – A Journey into the Nano World*, WILEY-VCH Verlag, Weinheim (2003).
- [29] V. Balzani, A. Credi, M. Venturi. *ChemSusChem*, **1**, 26 (2008).
- [30] C.A. Bignozzi, G.J. Meyer. In *Molecules as Components in Electronic Devices*, M. Lieberman (Ed.), ACS Symposium Series 844, pp. 154–170, American Chemical Society, Washington (2003).
- [31] J.K. McCusker. *Acc. Chem. Res.*, **36**, 876 (2003).
- [32] B.J. Coe, T.J. Meyer, P.S. White. *Inorg. Chem.*, **34**, 593 (1995).
- [33] B.P. Sullivan, D.J. Salmon, T.J. Meyer. *Inorg. Chem.*, **17**, 3334 (1978).
- [34] C.A. Bignozzi, S. Roffia, C. Chiorboli, J. Davila, M.T. Indelli, F. Scandola. *Inorg. Chem.*, **28**, 4350 (1989).
- [35] I. Evans, A. Spencer, G. Wilkinson. *J. Chem. Soc., Dalton Trans.*, 204 (1973).
- [36] B.J. Coe, M.C. Chamberlain, J.P. Essex-Lopresti, S. Gaines, J.C. Jeffery, S. Houbrechts, A. Persoons. *Inorg. Chem.*, **36**, 3284 (1997).
- [37] A. Vertova, I. Cucchi, P. Fermo, F. Porta, D.M. Proserpio, S. Rondinini. *Electrochim. Acta*, **52**, 2603 (2007).
- [38] I. Noviadri, K.N. Brown, D.S. Fleming, P.T. Gulyas, P.A. Lay, A.F. Masters, L. Phillips. *J. Phys. Chem. B*, **103**, 6713 (1999).
- [39] W. Kaim, J. Fiedler. *Chem. Soc. Rev.*, **38**, 3373 (2009).
- [40] *SCALE3 ABSPACK: Empirical Absorption Correction*, CrysAlis – Software package, Oxford Diffraction Ltd, Oxford (2006).
- [41] G.M. Sheldrick. *SHELXS97 and SHELXL97, Programs for Crystal Structure Resolution.*, University of Göttingen, Göttingen, Germany (1997).

- [42] F. Gajardo, A.M. Leiva, B. Loeb, A. Delgadillo, J.R. Stromberg, G.J. Meyer. *Inorg. Chim. Acta*, **361**, 613 (2008).
- [43] A. Cadranel, B.M. Aramburu Trošelj, S. Yamazaki, P. Alborés, V.D. Kleiman, L.M. Baraldo. *Dalton Trans.*, **42**, 16723 (2013).
- [44] J.G. Małecki, M. Jaworska, R. Kruszynski, R. Gil-bortnowska. *Polyhedron*, **24**, 1445 (2005).
- [45] W.-T. Wong, T.-C. Lau. *Acta Crystallogr., Sect. C*, **50**, 1406 (1994).
- [46] G.R. Desiraju. *Acc. Chem. Res.*, **35**, 565 (2002).
- [47] S. Alvarez. *Dalton Trans.*, **42**, 8617 (2013).
- [48] P. Metrangolo, G. Resnati, T. Pilati, R. Liantonio, F. Meyer. *J. Polym. Sci., Part A: Polym. Chem.*, **45**, 1 (2007).
- [49] D.S. Eggleston, K.A. Goldsby, D.J. Hodgson, T.J. Meyer. *Inorg. Chem.*, **24**, 4573 (1985).
- [50] P.S. Braterman, J.-I. Song. *J. Org. Chem.*, **56**, 4678 (1991).
- [51] M. Abe, Y. Sasaki, Y. Yamada, K. Tsukahara, S. Yano, T. Ito. *Inorg. Chem.*, **34**, 4490 (1995).
- [52] M. Abe, Y. Sasaki, Y. Yamada, K. Tsukahara, S. Yano, T. Yamaguchi, M. Tominaga, I. Taniguchi, T. Ito. *Inorg. Chem.*, **35**, 6724 (1996).
- [53] B.P. Sullivan, H. Abruna, H. Finklea, J.K. Nagle, T.J. Meyer, H. Sprintschnik. *Chem. Phys. Lett.*, **58**, 389 (1978).
- [54] B.J. Coe, M. Helliwell, M.K. Peers, J. Raftery, D. Rusanova, K. Clays, G. Depotter, B.S. Brunshwig. *Inorg. Chem.*, **53**, 3798 (2014).
- [55] B.J. Coe, J.A. Harris, L.A. Jones, B.S. Brunshwig, K. Song, K. Clays, J. Garin, S.J. Coles, M.B. Hursthouse. *J. Am. Chem. Soc.*, **127**, 4845 (2005).
- [56] B.P. Sullivan, D.J. Salmon, T.J. Meyer, J. Peedin. *Inorg. Chem.*, **18**, 3369 (1979).
- [57] R.M. Berger, D.R. McMillin. *Inorg. Chem.*, **27**, 4245 (1988).
- [58] P.S. Braterman, J.-I. Song, R.D. Peacock. *Spectrochim. Acta*, **48**, 899 (1992).
- [59] R.W. Callahan, F.R. Keene, D.J. Salmon, T. Meyer. *J. Am. Chem. Soc.*, **99**, 1064 (1977).
- [60] J.F. Endicott, H.B. Schlegel, J. Uddin, D.S. Seni. *Coord. Chem. Rev.*, **229**, 95 (2002).
- [61] S. Ardo, G. Meyer. *Chem. Soc. Rev.*, **38**, 115 (2009).
- [62] S. Campagna, S. Serroni, S. Bodige, F.M. MacDonnell. *Inorg. Chem.*, **38**, 692 (1999).
- [63] G. Denti, S. Serroni, S. Campagna, V. Ricevuto, V. Balzani. *Inorg. Chim. Acta*, **182**, 127 (1991).
- [64] F. Fagalde, N.E. Katz. *J. Chem. Soc., Dalton Trans.*, 571 (1993).
- [65] M. Cattaneo, F. Fagalde, C.D. Borsarelli, N.E. Katz. *Inorg. Chem.*, **48**, 3012 (2009).
- [66] E. Kosower, J. Cotter. *J. Am. Chem. Soc.*, **86**, 5524 (1964).